LA-UR -80-2525

TITLE: NONLINEAR RESPONSE OF A POST-TENSIONED CONCRETE STRUCTURE TO STATIC AND DYNAMIC INTERNAL-PRESSURE LOADS

AUTHOR(S): Thomas A. Butler, Q-13
Joel G. Bennett

SUBMITTED TO: Published in a special volume of the Journal of Computers and Structures for the ADINA conference to be held at the Massachusetts Institute of Technology June 10-12, 1981.

MASTER



University of California

LOS ALAMOS SCIENTIFIC LABORATORY
Post Office Box 1663 Los Alamos, New Mexico 87545
An Affirmative Action Equal Opportunity Employer

# NONLINEAR RESPONSE OF A POST-TENSIONED CONCRETE STRUCTURE TO STATIC AND DYNAMIC INTERNAL-PRESSURE LOADS

T. A. Butler
J. G. Bennett

Los Alamos Scientific Laboratory
Los Alamos, NM

---

## ABSTRACT

A nonlinear finite element model of a nuclear power plant containment building was developed to determine its ultimate pressure capability under quasistatic and impulsive dynamic loads. The ADINA finite element computer code was used to develop the model because of its capability to handle concrete cracking and crushing. Results indicate that, even though excessive concrete cracking occurs, failure is ultimately caused by rupture of post-tensioning tendons.

# NONLINEAR RESPONSE OF A POST-TENSIONED CONCRETE STRUCTURE TO STATIC AND DYNAMIC INTERNAL PRESSURE LOADS

T. A. Butler
J. G. Bennett

Los Alamos Scientific Laboratory
Los Alamos, NM

## I. INTRODUCTION

During a postulated meltdown accident in a pressurized water reactor (PWR), the containment building is the last line of defense for protecting the public from a release of fission products. Safety studies have indicated that the principal contributor to the risk of containment failure during a meltdown accident is overpressure generated by steam and noncondensable gases.[1] The overpressure loads are quasistatic in nature. A secondary risk contributor is an impulsive transient load generated by a hydrogen burn in the containment building. The purpose of this study was to set lower bounds for containment failure for both types of loads. Subsequently, a set point can be chosen for a pressure relief system for the containment building.

The specific containment building that we investigated is a lightly reinforced, post-tensioned concrete structure composed of a right circular cylinder and a spherical dome (Fig. 1). A massive transition ring between the cylinder and dome serves as an anchor for post-tensioning tendons. The interior of the building is lined with a 1/4 in.-thick (6.5-mm) ductile steel liner. The ultimate capability of the building is determined either by the pressure at which the steel liner separates, providing an escape path for fission products, or by failure of the post-tensioning tendons.

Because nonlinear and transient response calculations were required, we chose to study the problem with the ADINA finite element computer code[2] on the Los Alamos Scientific Laboratory (LASL) CRAY computer.

## II. CONTAINMENT BUILDING DESIGN

The containment building is a lightly reinforced, post-tensioned concrete structure with the basic dimensions shown in Fig. 1. Vertical post-tensioning in the cylindrical section is provided by 216 steel tendons anchored at the base slab on the bottom and the transition ring on the top. Post-tensioning in the hoop direction is provided by 579 tendons that each span 120°. These are anchored in six vertical buttresses evenly spaced around the building. All tendons are made of ninety 1/4-in.-(6-mm)-diam steel wires with an ultimate capacity of approximately 240 000 psi (1 660 MPa). The dome is post-tensioned by three groups of 63 tendons each, oriented at 120° with respect to each other. These tendons anchor to the cylinder-dome transition ring. Figures 2 and 3 show details of the cylinder intersection with the base slab and the dome and the tendon anchorages. When the building is constructed, the tendons are stressed to 80 % of their ultimate capability. They then perform at 60-65 % of their ultimate capability during the life of the structure.

The 1/4-in.-(6.4-mm)-thick steel liner is a leak-tight membrane made of ASTM A442 Grade 60 carbon steel. This type of steel has a nominal elongation of 23% in 2 in., so the concrete to which it is anchored will have to crack considerably and the associated steel reinforcement will have to yield to allow the liner to stretch enough to fail. Even though the steel is ductile, some caution must be used when evaluating its response because it is in a biaxial stress state and the ductility can be lower near discontinuities (i.e., anchor points) and weld seams.

The building was designed to withstand an internal quasistatic pressure of 47 psig (0.32 MPa) with two basic design criteria. The first was to guarantee the integrity of the liner plate under all loading conditions. Second, the structure is to have a low-strain, elastic response such that its behavior may be completely predictable under the required loadings.

## III. STRUCTURAL MODELING

The containment building analyzed here is not a truly axisymmetric structure because of the buttresses that run vertically from the transition ring to the base mat every 60°. Also, the tendon arrangement in the dome has only periodic symmetry and is not truly axisymmetric. Although it is an obvious simplication, we chose to model the containment building as an

axisymmetric structure because of its near symmetry. An axisymmetric model is also a logical choice because of size requirements for running nonlinear and dynamic analyses. The quasistatic overpressure loads are naturally axisymmetric. The impulsive transient pressure loads generated by a hydrogen burn are not necessarily axisymmetric. However, the choice of any other loading distribution would be somewhat arbitrary. So, again, axisymmetric loading was chosen for our initial studies.

Before we determined the mesh for the ADINA model, we developed a simple linear model of the structure with an interactive linear finite element code.[3] Data from this analysis, primarily internal load distributions, not only helped in developing an optimum mesh, but provided valuable data for checking our ADINA calculations and understanding the results. Figures 4 and 5 show the internal moment distributions for the cylindrical and dome sections of the building for certain loads and load combinations. In the figures the moments are given as (in. - kip)/in. where 1 kip is equal to 1000 lbs (4 448 N). From the linear combination of the post-tensioning moments and the moments due to an internal pressure of 47 psig (0.32 MPa), we can determine that moment reversal occurs at the top of the cylindrical section at approximately 70 psig (0.48 MPa) internal pressure. Moment reversals occur at other key locations at higher pressures. These pressures are important because the steel reinforcement in the concrete is located preferentially to take maximum moments from post-tensioning with no internal pressure. Even at the design accident pressure of 47 psig (0.32 MPa), these moments are lower and of the same sign. When moment reversal occurs, the structure is no longer in a design load state.

The philosophy of the nonlinear axisymmetric model was to have a fairly accurate representation of the concrete and steel in the sidewall high moment regions and in the dome. ADINA was chosen for the finite element analyses because it met nearly all requirements for both static and dynamic analyses with the exception of having an axisymmetric shell element in its element library. A nonlinear two-dimensional shell element had previously been developed and tested at LASL[4] for inclusion in the ADINA element library, and was implemented into the CRAY version of the code for this analysis. The mesh shown in Fig. 6 was developed using the [illegible] code described in Ref. 5 so that eventual mesh refinement could be easily carried out. For an accuracy assessment, this mesh refinement is considered to be a necessary step.

The concrete material model used is the tensile cracking, compression crushing, strain softening model described in Ref. 6. The tensile cracking mechanism is implemented by examining the maximum principal stress at each element integration point. If this stress exceeds the uniaxial cutoff tensile stress, a failure plane (interpreted here as a "cracked" plane) has formed normal to the maximum principal stress direction. The normal stiffness across this plane is decreased to a user-specified factor times the original stiffness. The shear stiffness at this integration point is similarly reduced. We used the 8-node isoparametric axisymmetric element with a 3 x 3 array of integration points. A normal stiffness reduction factor of 0.000 1 and a shear stiffness reduction factor of 0.5 were used. Table I summarizes the concrete material properties. We used the same triaxial compressive failure envelope given in Ref. 6.

The meridional sidewall tendons were modeled using three prestrained truss elements for each tendon. These tendons run from the ring top anchor points to the dome spring line, from the spring line to the break in thickness in the sidewall, and from this point to the base mat anchor point. Two sidewall tendon sets were modeled in the wall interior with the area of each set specified to be one-half the total tendon area in a one radian segment of the actual structure.

The meridional dome tendons were modeled with the prestrained trusses passing through the center of the dome elements and anchored at the ring exterior. Each truss has a different area calculated based on its particular position in the dome, with the area being the full area in a one radian segment of the actual structure for the tendons running parallel to the meridional coordinate plus the projected area of both tendon sets within the one radian segment crossing at $60^{0}$ to the meridian.

The hoop tendons on the sidewall exterior were modeled with prestrained "ring" trusses of varying area such that the tendon area at each exterior wall node was based on the distance between nodal points in the model and the tendon area in the actual structure. Dome hoop tendons were similarly modeled using prestrained ring trusses. The area of the tendons crossing the meridian in the one radian segment was projected into the hoop direction. All tendons were specified to have an initial strain of 0.7, a yield stress of $2.16 \times 10^{5}$ psi (1.49 GPa), [illegible] stress of $2.11 \times 10^{5}$ psi (5.59 GPa). The [illegible]

TABLE I

CONCRETE MATERIAL PROPERTIES

| | |
|---|---|
| Tangent modulus of elasticity at zero strain | $5 \times 10^6$ psi (35 GPa) |
| Poisson's ratio | 0.2 |
| Uniaxial cutoff tensile stress | 500 psi (3.5 MPa) |
| Uniaxial maximum compressive stress | 5 500 psi (38 MPa) |
| Corresponding uniaxial compressive strain | 0.002 |
| Uniaxial ultimate compressive stress | 4 000 psi (28 MPa) |
| Corresponding ultimate compressive strain | 0.003 |

elements after equilibrium is established for this initial strain varies from about 147 000 psi (1.01 GPa) to 154 000 psi (1.06 GPa), which is 61-64 % of their ultimate strength. This value of post-tensioning is consistent with that in the actual structure.

Reinforcement in the containment building is ASTM A-432 steel with a yield strength of 60 000 psi (414 MPa). In the cylindrical and spherical dome sections we represented the steel reinforcement with ring and truss finite elements. In the base slab, where the effect of the steel is not so critical, we modeled the reinforcement more simplistically with shell finite elements. All of the reinforcement is located on the inner and outer node points of the mesh (Fig. 6). For both cases, the steel is constrained to move with the concrete at each node point simulating a perfect bond. However, between node points, displacement compatibility between the concrete and truss and ring elements does not exist.

The 1/4-in. (6-mm) steel liner on the interior of the structure is modeled with the axisymmetric nonlinear shell element described in Ref. 4. Young's modulus in the elastic region is specified to be $30 \times 10^6$ psi (210 GPa). The yield strength is 32 000 psi (220 MPa) with a tangent modulus of 165 000 psi (1.14 GPa).

Boundary conditions used for the model are shown in Fig. 6. For this study, the effect of the soil pressure on the outside of the lower portion of the cylindrical wall was neglected. Also, while the static test described in Ref. 7 indicates a slight amount of base slab uplift, we judged that the failure pressure and mode of failure would not be significantly influenced if this boundary is assumed to be fixed. Several other model limitations are as follows:

- Axisymmetric modeling of a structure that is only nearly axisymmetric.
- Building penetrations are not modeled.
- Internal structure and heavy equipment are not represented.
- Tendons are only approximately modeled with the truss representation, particularly on the dome region where trusses are tied to each concrete element for proper curvature.
- The actual liner anchor spacing is not represented; rather the liner is attached to the concrete at each interior node.

None of these limitations is deemed serious enough to preclude an appropriate assessment of the ultimate load carrying capacity of the building.

## [illegible] EXPERIMENTAL EVIDENCE

Structural integrity tests performed on the containment building and reported in Ref. 7 provide a source of experimental data with which the model results can be compared. The structural integrity test involves a pressurization of the containment building to 54 psig followed by depressurization. Selected displacement data and crack surveys were made during this test. Figure 7 shows the locations of the extensometers used to measure radial displacement of the sidewall and vertical displacement of the dome relative to the operating floor. The ADINA model was loaded first with the gravity loading plus the tendon preload. Figure 8 shows the maximum principal stress contours in the ring region from this loading. Local compressive regions indicative of the tendon anchor points for both sidewall tendons and dome tendons can be readily identified.

Next, an internal pressure of 54 psig was applied to the finite element model and the displacements of the nodes closest to the gauge locations were used for comparison purposes. Table II shows the ADINA model predictions and measured response. Deviations can be attributed to a number of causes including measurement error, the material property assumptions for concrete, and the approximations made in the finite element modeling. Figure 9 shows the maximum principal stress contours in the liner at the elevation for this case, (1.0 x PIL + 54 psig), where PIL stands for prestressing load. Comparison of Fig. 8 with 9 indicates that the [illegible] tension has shifted to an area higher on the ring. [illegible]

tension, indicating the sign of the bending moment there is still in the sense for which the structure was designed.

TABLE II
ADINA MODEL COMPARED TO 54 psig TEST RESULTS

| Gauge | Measured (in.) | Prediction (in.) | Deviation (in.) |
|---|---|---|---|
| | Radial Displacement of Cylinder Wall | | |
| R1 | 0.07 | 0.05 | + 0.02 |
| R2 | 0.16 | 0.16 | + 0.02 |
| R3 | 0.14 | 0.16 | - 0.02 |
| R4 | 0.14 | 0.17 | - 0.03 |
| R5 | 0.05 | 0.07 | - 0.02 |
| | Vertical Displacement of Dome from Operating Floor | | |
| D1 | 0.38 | 0.35 | + 0.03 |
| D2 | 0.42 | 0.34 | + 0.08 |
| D3 | 0.21 | 0.18 | + 0.03 |

Note: Positive deviation indicates the measured displacement is greater than the predicted response.

## V. STATIC RESPONSE

The load-step history shown in Fig. 1c was applied to the model to determine the ultimate capacity of the structure. Figure 11 shows the maximum principal stress contours in the [illegible] at load step 2 (1.0 g + PTL + 87 psig). Note that the [illegible] shifted to the interior surface of the [illegible]. In addition, the interior sidewall now has larger tensile [illegible], indicating moment sign reversal has occurred, a situation for which the building presumably was not designed. Figure 12 [illegible] step 3, 1.0 + PTL + 91 psig, the [illegible]

that magnitudes are approaching the maximum allowable tension in the concrete on the inner surface. Between 91 and 92 psig, ADINA indicates that the concrete cracks on the inner surface of the ring (Fig. 13). Figure 14 illustrates the new distribution of maximum tensile stress as tensile stresses in the concrete are relieved. The maximum tensile areas now redistribute to either side of the cracked region. Equilibrium is maintained by the steel reinforcing and the liner. For example, the stress level in the shell used to define material yield goes from 4 000 psi (28 MPa) before cracking to 17 000 psi (117 MPa) immediately after cracking. This stress level is equal to three times the second invariant of the stress deviator for a biaxial stress state.

The calculation continued essentially unchanged to 96 psig (0.66 MPa) with no further cracks developing. Between 96 psig (0.66 MPa) and 97 psig (0.67 MPa), a large part of the central portion of the cylindrical sidewall cracks in the hoop direction. This cracking is caused by the large membrane loads in the wall. When the wall cracks, the load previously carried in the concrete is transferred to the steel reinforcement and post-tensioning tendons, considerably increasing the loads that they carry. The gross cracking of the wall also changes the internal load distribution in the structure enough to cause cracking from bending stresses at both sides of the dome transition ring and near the bottom of the cylindrical sidewall (72 in. (1.8 m) from its intersection with the base slab).

Except for a few cracks closing in one element in the transition ring, the calculation remains unchanged in character to 103 psig (0.71 MPa). At this internal pressure, the steel liner near the middle of the sidewall yields because of high strains in the hoop direction. Even though the liner yields, it should remain intact because of its relatively high ductility until the steel reinforcement in the wall yields. Once the reinforcement yields, the concrete can separate, stretching the liner and allowing significant shear deflections in the concrete and thus the liner. During the pressure load history, the stresses in the hoop reinforcement and tendons steadily increase but remain below the material yield points.

Between 103 psig (0.71 MPa) and 112 psig (0.77 MPa), the concrete develops a few additional cracks in the high moment regions. However, no yielding of the reinforcement has occured so all crack openings remain small

and the steel liner is still intact though yielded at the cylindrical sidewall. At a pressure of slightly over 112 psig (0.77 MPa), the calculation experiences a numerical instability. This can probably be attributed to additional cracking of concrete, causing some previously developed cracks to close. Examinations of maximum principal stresses in the concrete at 112 psig (0.77 MPa) reveals imminent cracking at several locations. In particular, an element near the base of the wall will crack at several integration points before an additional 0.1 psig (690 Pa) is applied.

Because the structure has not reached its failure point, based on steel reinforcement and tendon stresses, we linearly extrapolated the ADINA stresses in key elements to approximate the most likely failure pressures for different failure modes. Table III presents the failure modes along with an approximation of the maximum pressure for each mode. These estimates have excluded the possibility that additional cracking of the concrete will radically change the loads in the reinforcement and tendons that are most likely to fail. This is a good approximation, especially because the first failure mode comes from membrane induced stresses that are not likely to change with additional concrete cracking.

TABLE III

PREDICATED FAILURE MODES AND PRESSURES

| Failure Mode | Pressure |
|---|---|
| Tendon yield from excessive membrane loads in hoop direction. | 120 psig (0.83 MPa) |
| Liner failure from excessive concrete cracking accompanied by reinforcement yield. | |
| Base of cylindrical wall | [illegible] MPa) |
| Dome transition ring | [illegible] MPa) |

## VI. DYNAMIC RESPONSE

To assess the response of the containment structure to a hydrogen explosion, we performed a dynamic analysis u ing the model described above. The transient time history shown in Fig. 15 was applied as a pressure loading to the entire interior (no spatial variation) of the containment. This transient represents a 100 psig (0.7 MPa) peak pressure impulse that could arise from a hydrogen burn followed by a long time overpressure thermal effect. Calculations were also carried out with a 200 psig (1.4 MPa) peak pressure dynamic load.

To help explain the calculated transient response, we obtained the first five axisymmetric modes of vibration for the structure along with their frequencies. The mode shapes and frequencies are shown in Fig. 16. The fundamental, or lowest frequency, is 12.1 Hz and the mode shape involves the massive dome ring moving with high bending regions to either side of it in the cylinder wall and the dome. These modes were obtained with the structure in its configuration before post-tensioning. With the post-tensioning effects present, the frequencies are expected to be somewhat lower. Also, the modal data are exactly applicable only when the structural response is linear. As the concrete cracks or crushes and the steel yields, these frequencies will be even lower.

Figure 17 shows the displacement response of the dome apex for the first 125 ms of building response to the 100 psig (0.7 MPa) pressure transient described above. The apex translates vertically $\pm$ 1.2 in. (30 mm) from its equilibrium point of -0.6 in. (15 mm). Frequency of response is dominated by a mode with an apparent frequency of approximately 8 Hz. This is probably the fundamental mode with its frequency lowered by the post-tensioning and concrete cracking effects. In the model, we do not account for any structural damping other than that coming from nonlinear material effects. In reality, there is probably 7-10% equivalent viscous damping for a structure of this sort. If this damping were considered, the response would be somewhat lower through the first cycle of the fundamental frequency.

Cracking of the concrete from this transient is severe. Figures 18 and 19 show the developing crack pattern at the dome-ring intersection. The first crack plane in the structure appears at time T = 10.1 ms as shown in Fig. 18. By time T = 11.5 ms, the entire region is cracked in the manner shown in Fig. 19. In general, during the transient response, most of the

structural concrete has undergone cracking, though many cracks close again to carry compressive loading. Figure 20 illustrates the severity of the cracking in the intersection region of the side wall and base slab. The concrete in this region at time T = 40 ms has cracked completely through the wall. Reinforcement strains at this time are small, however, indicating that the structure does not undergo shear failure.

The region near the apex not only cracks during the transient, but also undergoes a compressive crushing failure. For the concrete material model that we used, this means the material no longer will carry load. It should again be noted that we have made the reinforcement axisymmetric in the model, whereas in the actual structure the reinforcement distribution is not axisymmetric. This simplification could influence this mode of failure and should be studied in some future analysis. Figure 21 shows the crushed region at the apex of the dome.

The reinforcement remains elastic throughout the transient, indicating that though severe damage to the concrete occurs, the load carrying ability of the structure remains.

The liner undergoes yield during the transient in the two regions indicated on Fig. 21. The peak strains, however, remain below 0.13-0.14%. Because of the large ductility of the liner material (23%), the liner will not be breached, though further investigation of local strains near liner anchors and more refined modeling are needed to resolve this question.

In general, the finite element model indicates that this transient will damage the building beyond repair. However, the ability of the liner to maintain the internal overpressure remains. A repeat of the calculation with a 200 psi peak pressure indicated catastrophic failure of the containment building because several tendons reach their ultimate load carrying capacity.

## VII. CONCLUSIONS

For a static or quasistatic loading condition the containment building concrete will first begin to crack at the transition ring between the cylindrical walls and spherical dome at 92 psig (0.63 MPa). Cracking continues to 112 psig (0.77 MPa) where a calculational instability occurs. From this point, linear extrapolations of ADINA results indicate that the structure's ultimate pressure capability is 120 psig (0.83 MPa), with the first failure

mode being rupture of hoop tendons near the midpoint of the cylindrical side wall. For the dynamic loading used in the 100 psig (0.7 MPa) peak calculation, the containment capability will remain but the concrete will be damaged beyond repair. We also applied a 200 psig (1.4 MPa) peak impulse to this model. Although we did not run the calculation long enough to obtain the peak building response, early time results predict catastrophic failure of the structure.

REFERENCES:


1. D. D. Carlson and J. W. Hickman. A value-impact assessment of alternate containment concepts. Sandia Laboratories report SAND77-1344 (NUREG/CR-0165), June 1978.

2. K. J. Bathe. ADINA: A finite element program for automatic dynamic incremental nonlinear analysis. MIT report 82448-1, Sept. 1975 (revised Dec. 1978).

3. W. D. Whetstone. SPAR structural analysis system reference manual. NASA report NASA-CR-145098-1, Vol. I (February 1977).

4. W. A. Cook. Linear and nonlinear symmetrically loaded shells of revolution approximated with the finite element method. Los Alamos Scientific Laboratory report LA-7538-MS (October 1978).

5. W. A. Cook. INGEN: A general-purpose mesh generator for finite element codes. Los Alamos Scientific Laboratory report LA-7135-MS (February 1978).

6. K. J. Bathe and S. Ramaswamy. On three-dimensional nonlinear analysis of concrete structures. Nuc. Eng. and Design 52, 385-409 (1979).

7. Structural response of the containment structure of the Zion Nuclear Plant Unit No. 1 during structural integrity tests -- Commonwealth Edison Company. For Sargent and Lundy (submitted by Wiss, Janney, Elstner, and Associates, Inc.) (March 1973).

NONLINEAR RESPONSE OF A POST-TENSIONED CONCRETE....

T. A. Butler
J. G. Bennett
Los Alamos Scientific Laboratory

FIGURE CAPTIONS

Fig. 1 Containment building.

Fig. 2 Details of cylinder-base slab intersection.

Fig. 3 Details of cylinder-dome intersection.

Fig. 4 Moment distributions in cylindrical portion of containment.

Fig. 5 Moment distribution in dome portion of containment building.

Fig. 6 ADINA finite element model of containment building.

Fig. 7 Displacement gauge locations.

Fig. 8 Maximum principal stress contours in transition ring with 1 g plus post-tensioning loads.

Fig. 9 Maximum principal stress contours in transition ring with 54 psig (0.38 MPa) internal pressure.

Fig. 10 Static load step history applied to ADINA finite element model.

Fig. 11 Maximum principal stress contours in transition ring with 87 psig (0.60 MPa) internal pressure.

Fig. 12 Maximum principal stress contours in transition ring with 91 psig (0.63 MPa) internal pressure.

Fig. 13 Initial crack pattern at 92 psig (0.63 MPa).

Fig. 14 Maximum principal stress contours in transition ring with 97 psig (0.63 MPa) internal pressure.

Fig. 15 Pressure transient applied to ADINA finite element model.

Fig. 16 First five mode shapes of dynamic model.

Fig. 17 Transient response of dome apex to 100 psig (0.7 MPa) peak pressure pulse.

Fig. 18 Crack pattern development at the dome-transition ring intersection to 10.6 ms.

Fig. 19 Crack pattern development at the dome-transition ring intersection to 12 ms.

Fig. 20 Crack pattern at the [illegible] wall-base [illegible] ms.

Fig. 21 Liner and concrete response to 100 psig [illegible] pressure transient.

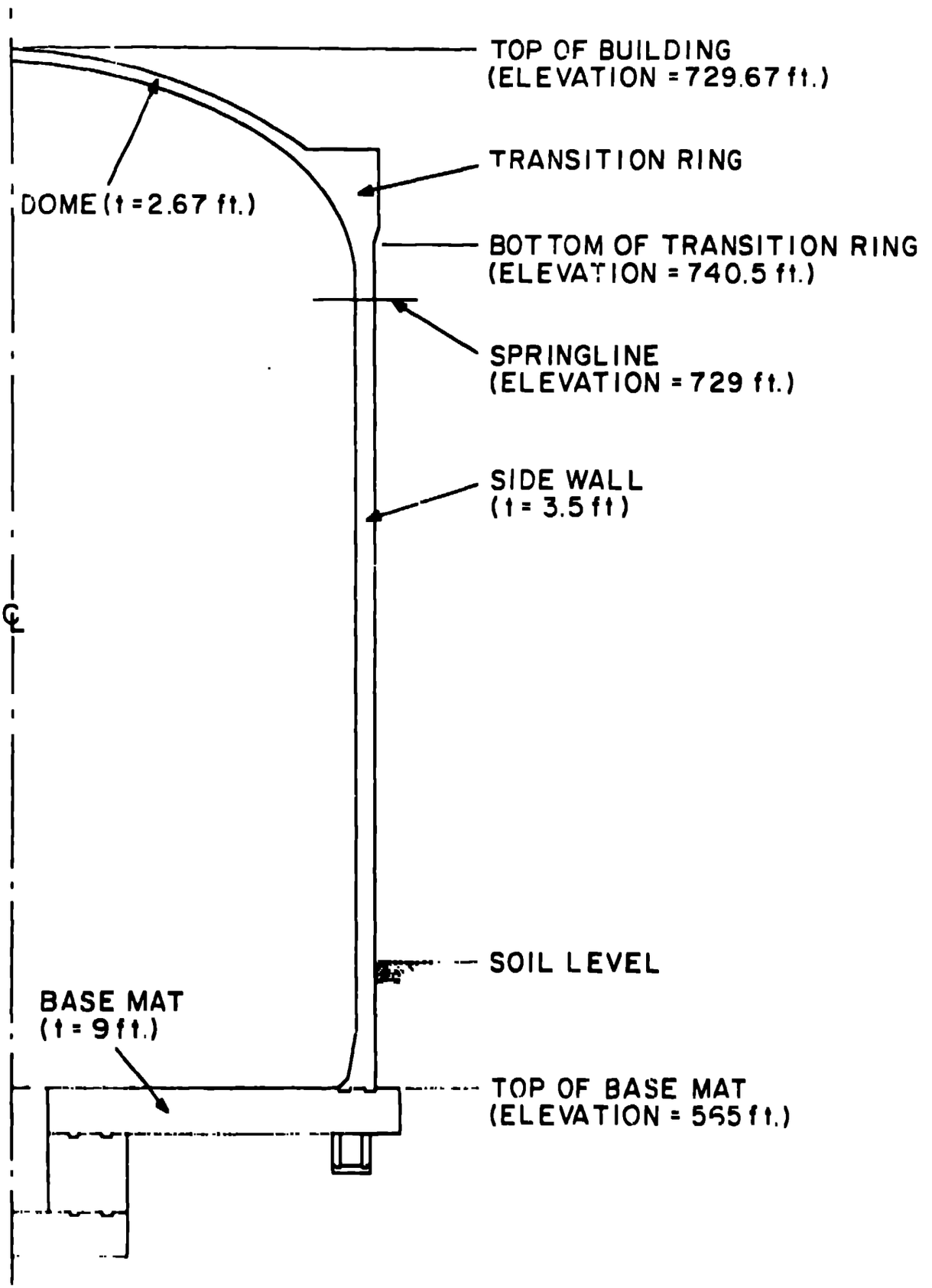
TOP OF BUILDING
(ELEVATION = 729.67 ft.)
TRANSITION RING
DOME (t = 2.67 ft.)
BOTTOM OF TRANSITION RING
(ELEVATION = 740.5 ft.)
SPRINGLINE
(ELEVATION = 729 ft.)
SIDE WALL
(t = 3.5 ft)
℄
SOIL LEVEL
BASE MAT
(t = 9 ft.)
TOP OF BASE MAT
(ELEVATION = 565 ft.)

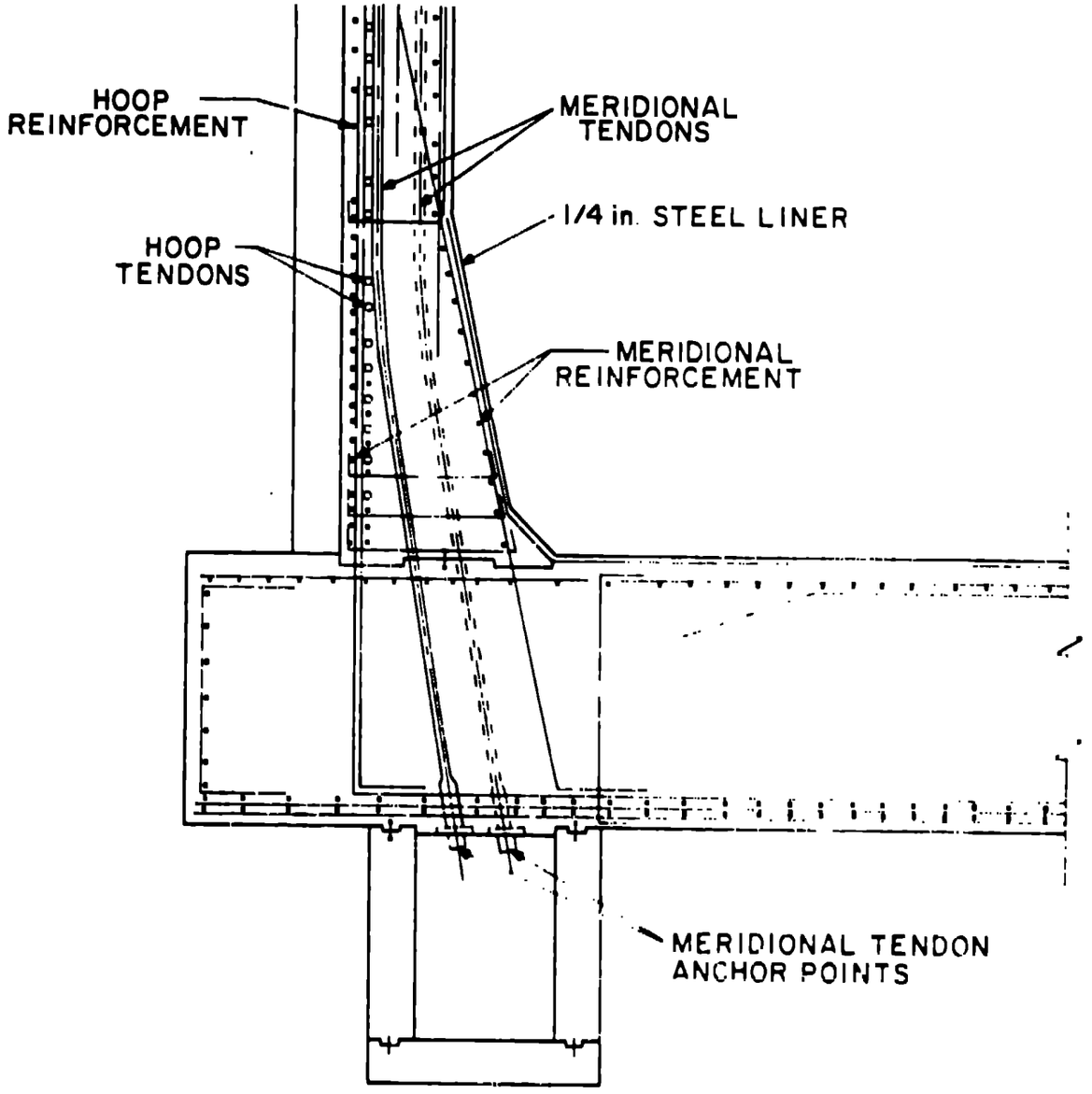
HOOP
REINFORCEMENT
MERIDIONAL
TENDONS
1/4 in. STEEL LINER
HOOP
TENDONS
MERIDIONAL
REINFORCEMENT
MERIDIONAL TENDON
ANCHOR POINTS

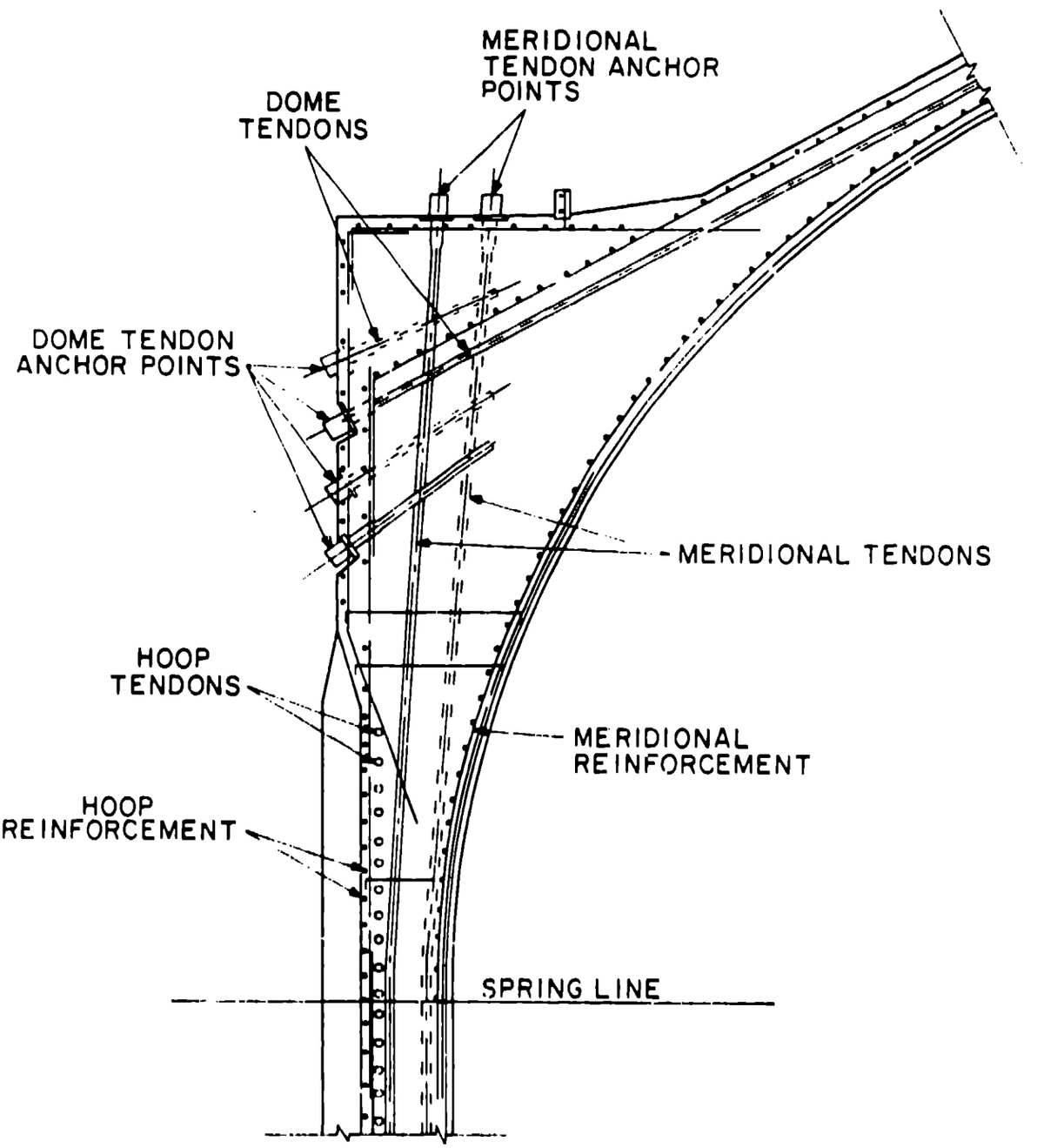
MERIDIONAL
TENDON ANCHOR
POINTS
DOME
TENDONS
DOME TENDON
ANCHOR POINTS
MERIDIONAL TENDONS
HOOP
TENDONS
MERIDIONAL
REINFORCEMENT
HOOP
REINFORCEMENT
SPRING LINE

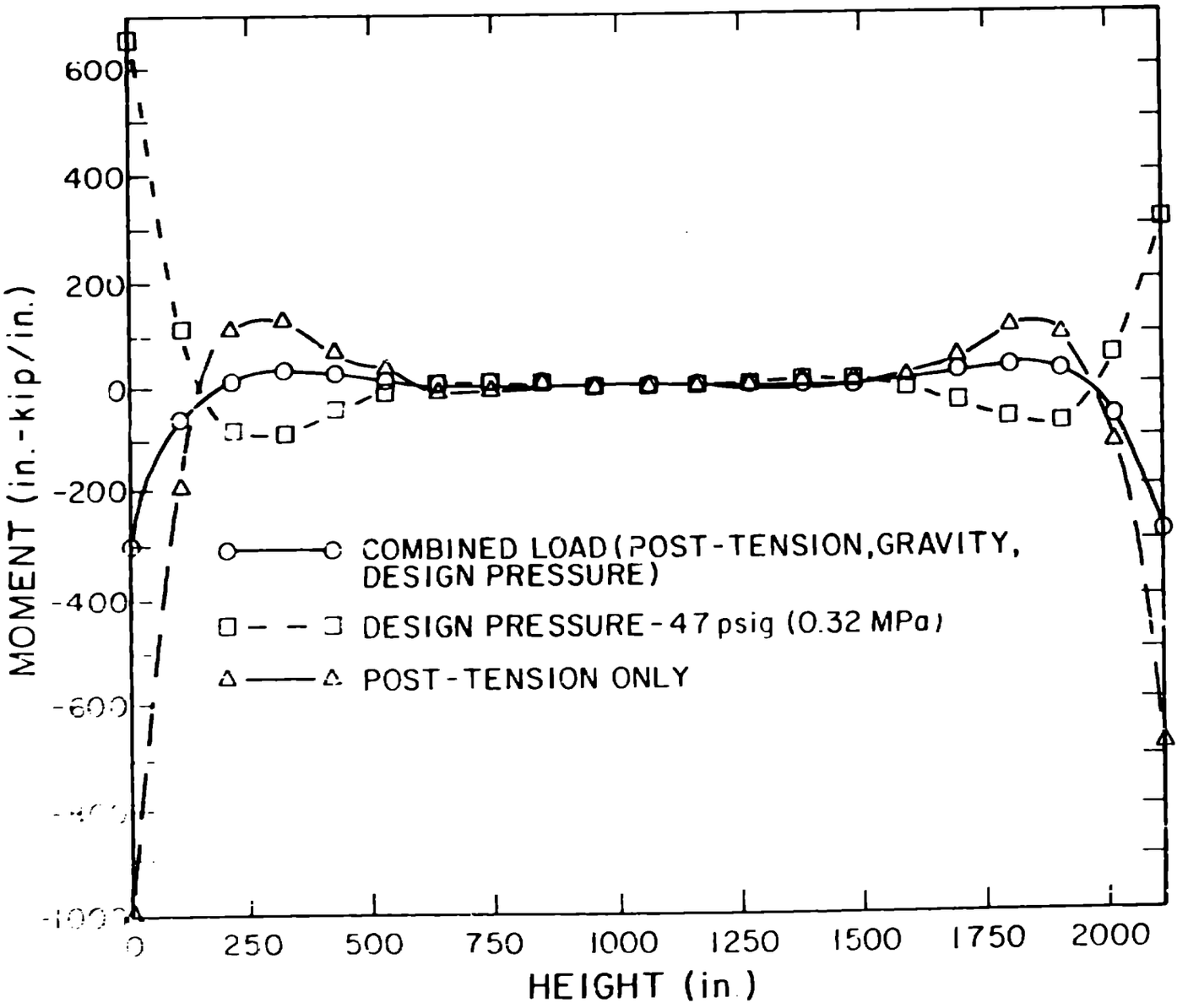
MOMENT (in.-kip/in.)
600
400
200
0
-200
-400
-600
0
250
500
750
1000
1250
1500
1750
2000
HEIGHT (in.)
COMBINED LOAD (POST-TENSION, GRAVITY, DESIGN PRESSURE)
DESIGN PRESSURE - 47 psig (0.32 MPa)
POST-TENSION ONLY

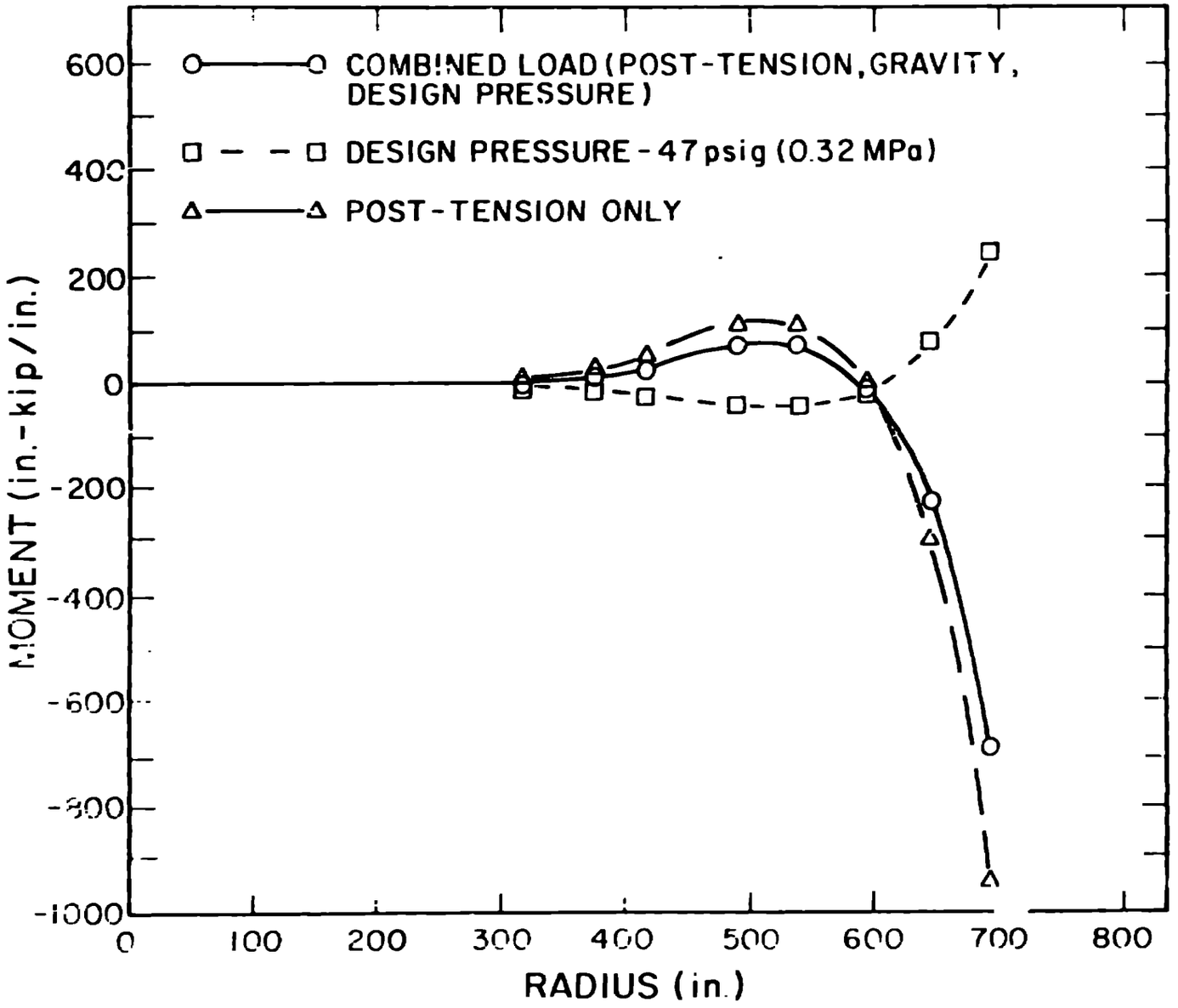
COMBINED LOAD (POST-TENSION, GRAVITY, DESIGN PRESSURE)
DESIGN PRESSURE - 47 psig (0.32 MPa)
POST-TENSION ONLY
MOMENT (in.-kip/in.)
600
400
200
0
-200
-400
-600
-800
-1000
0
100
200
300
400
500
600
700
800
RADIUS (in.)

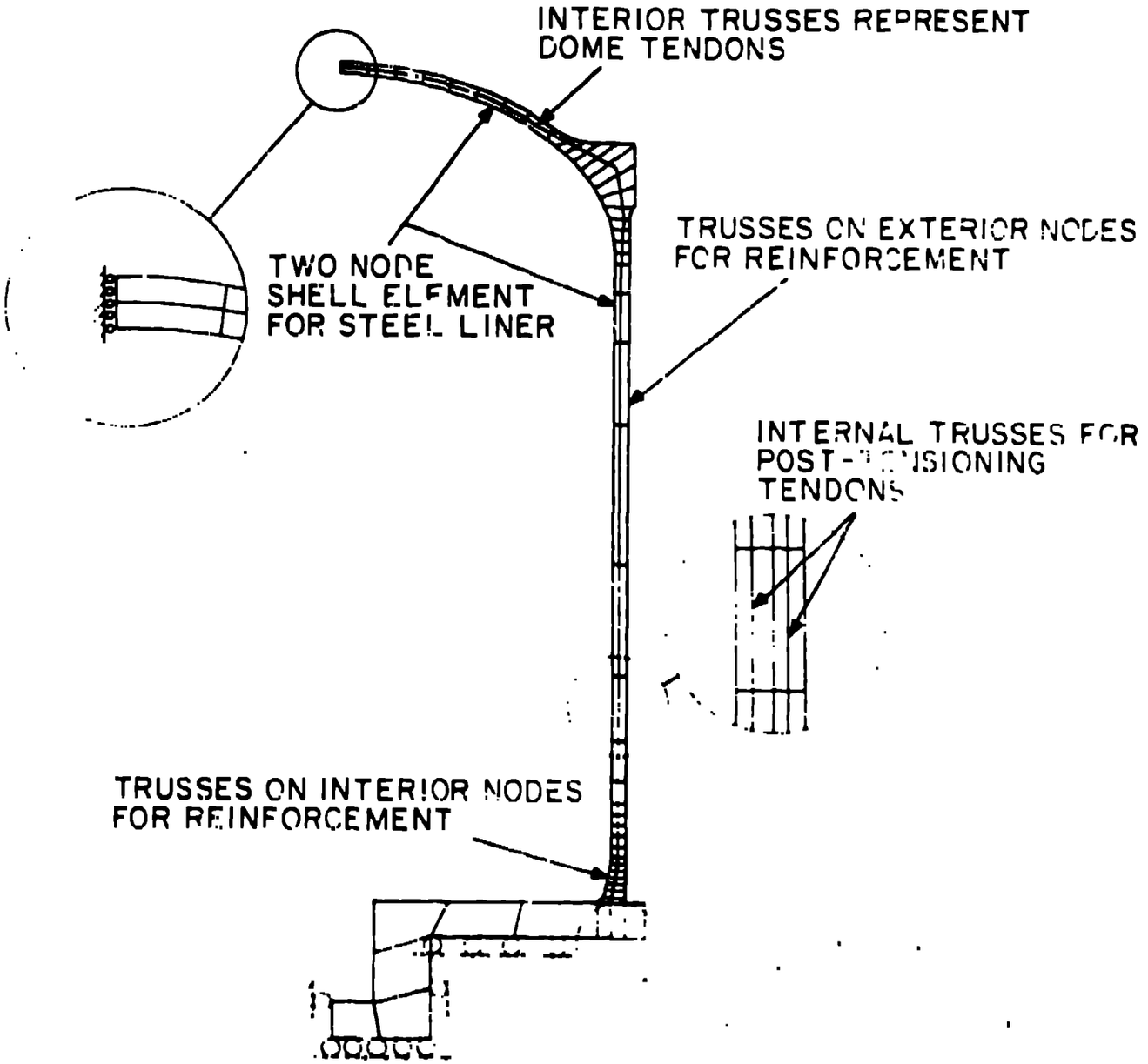
INTERIOR TRUSSES REPRESENT
DOME TENDONS
TRUSSES ON EXTERIOR NODES
FOR REINFORCEMENT
TWO NODE
SHELL ELEMENT
FOR STEEL LINER
INTERNAL TRUSSES FOR
POST-TENSIONING
TENDONS
TRUSSES ON INTERIOR NODES
FOR REINFORCEMENT

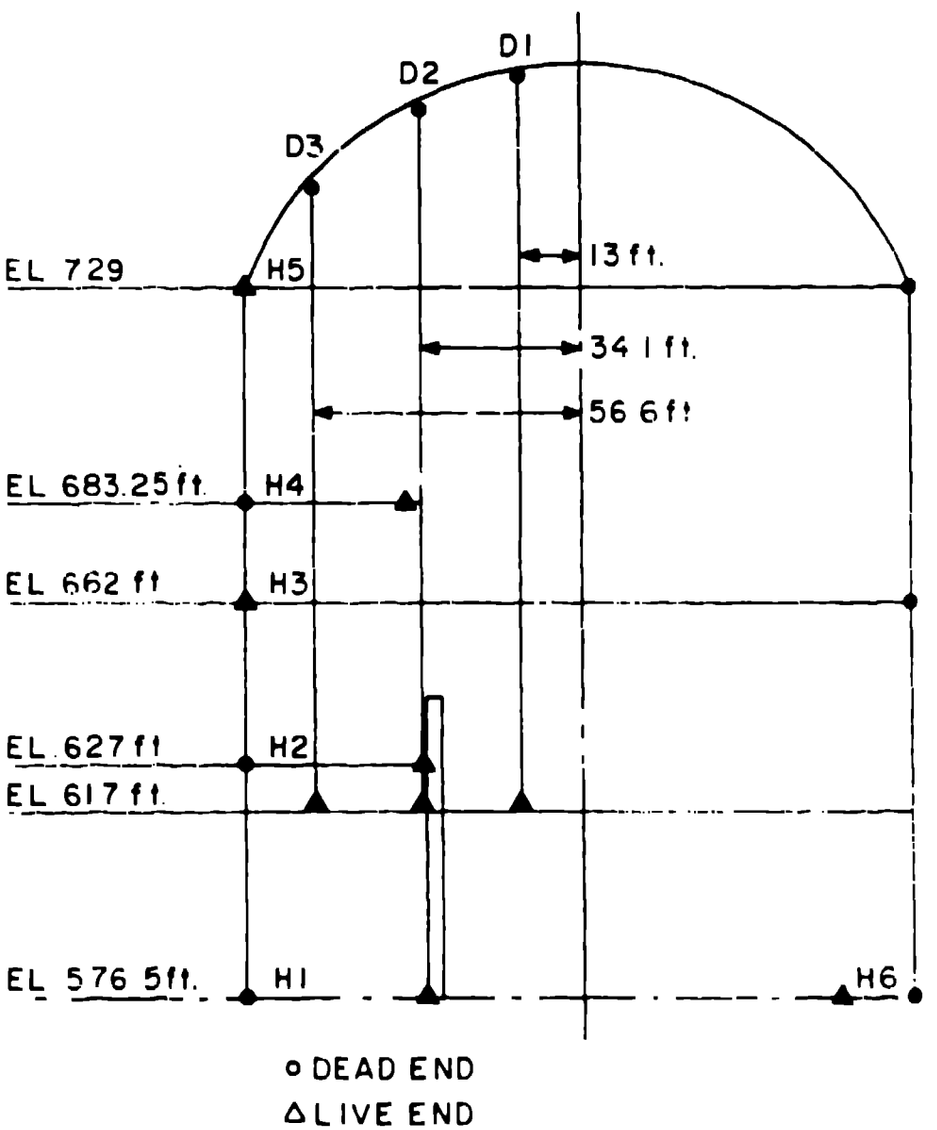
D1
D2
D3
EL 729
H5
13 ft.
34 1 ft.
56 6 ft
EL 683.25 ft.
H4
EL 662 ft
H3
EL 627 ft
H2
EL 617 ft.
EL 576 5ft.
H1
H6
o DEAD END
Δ LIVE END

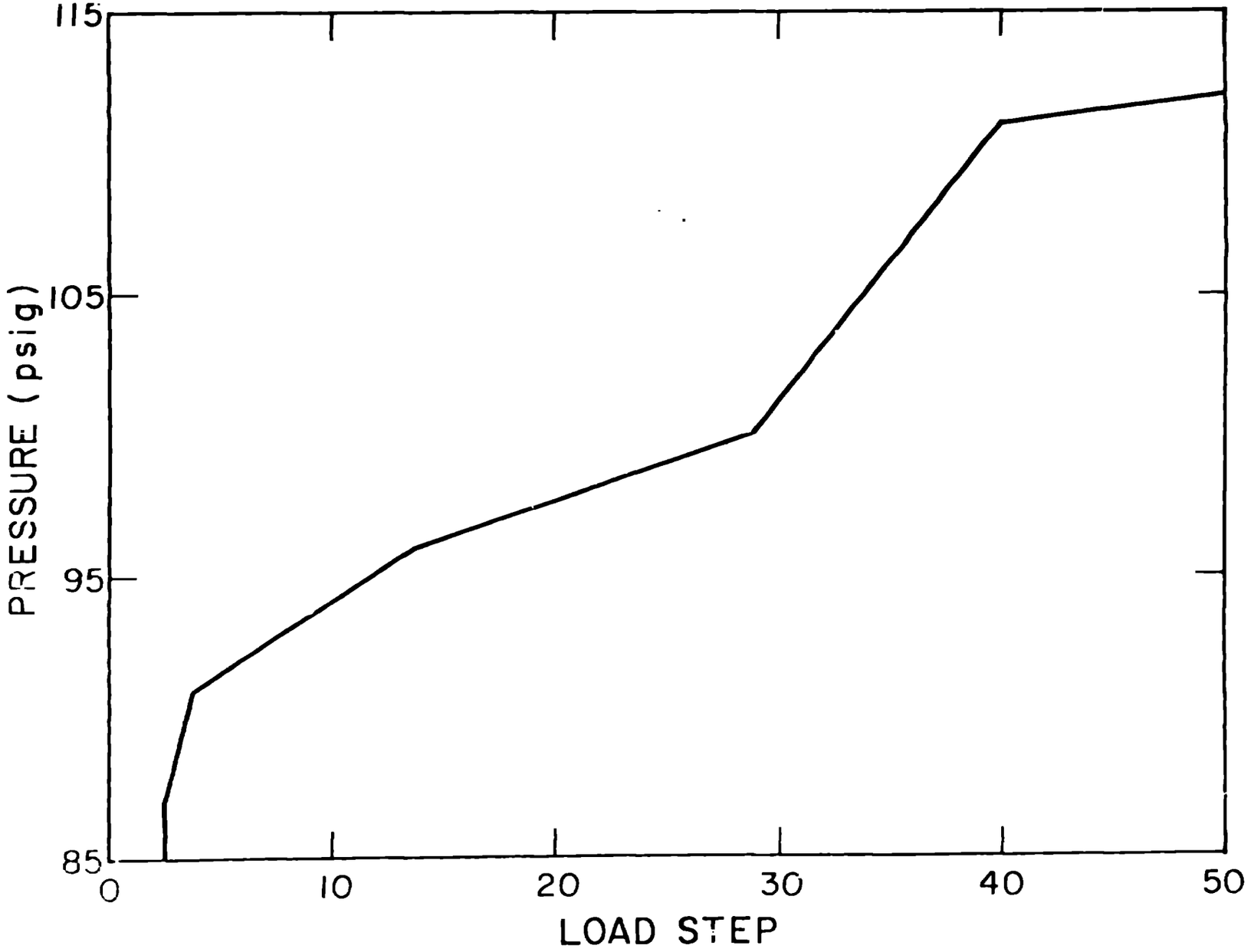
115
105
95
85
PRESSURE (psig)
0
10
20
30
40
50
LOAD STEP

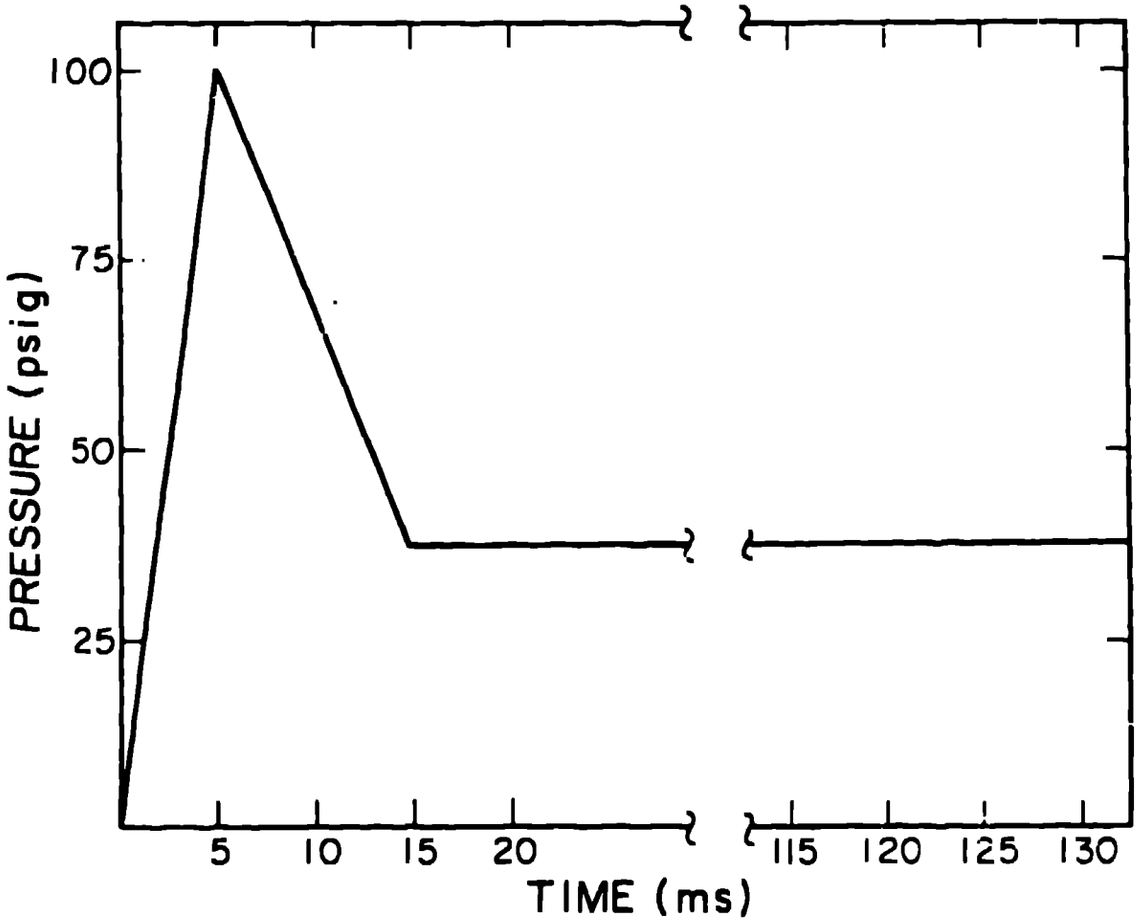
100
75
50
25
PRESSURE (psig)
5
10
15
20
115
120
125
130
TIME (ms)

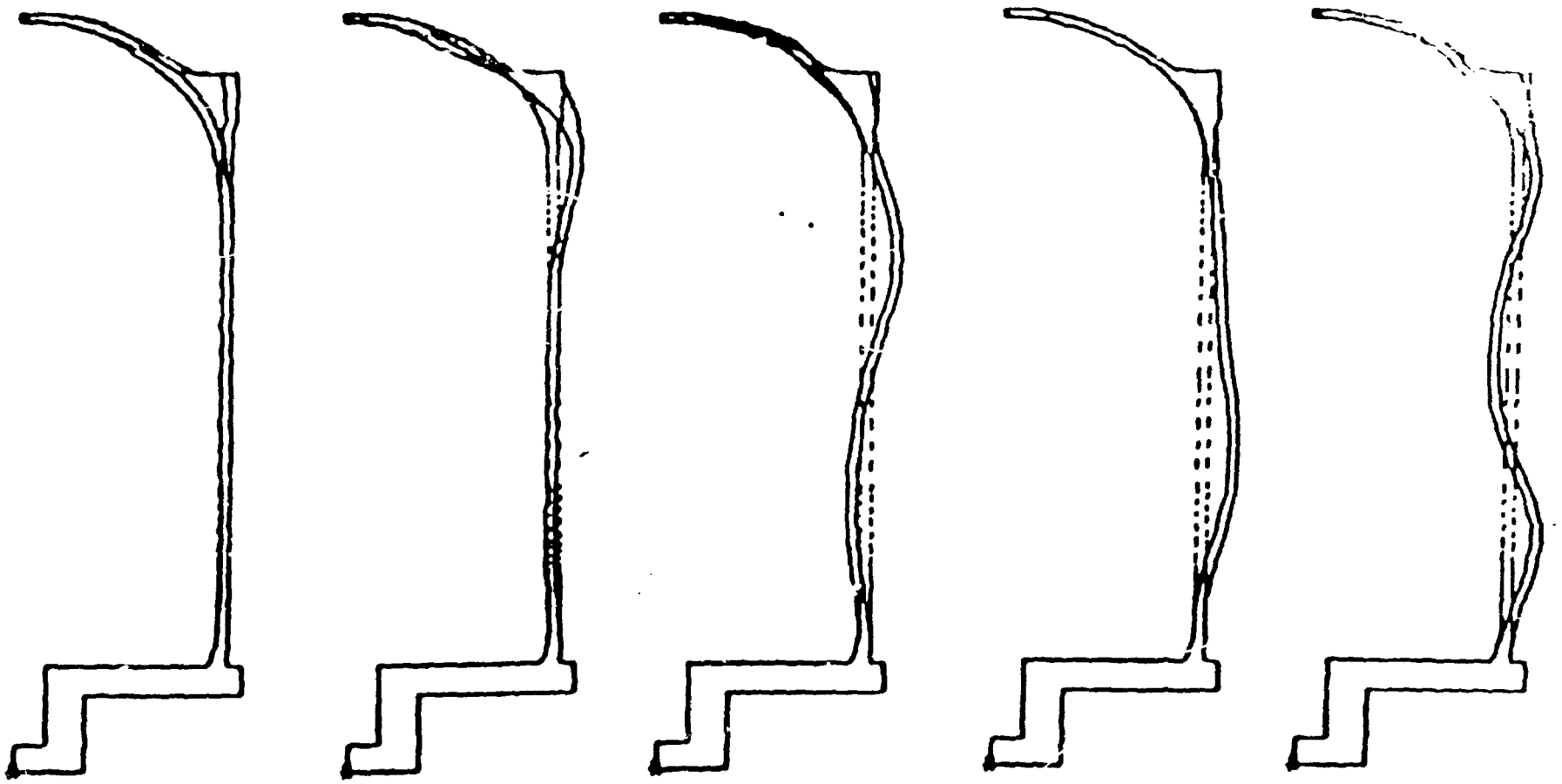

12.1 21.2 24.2 27.5 28.5

(Hz)

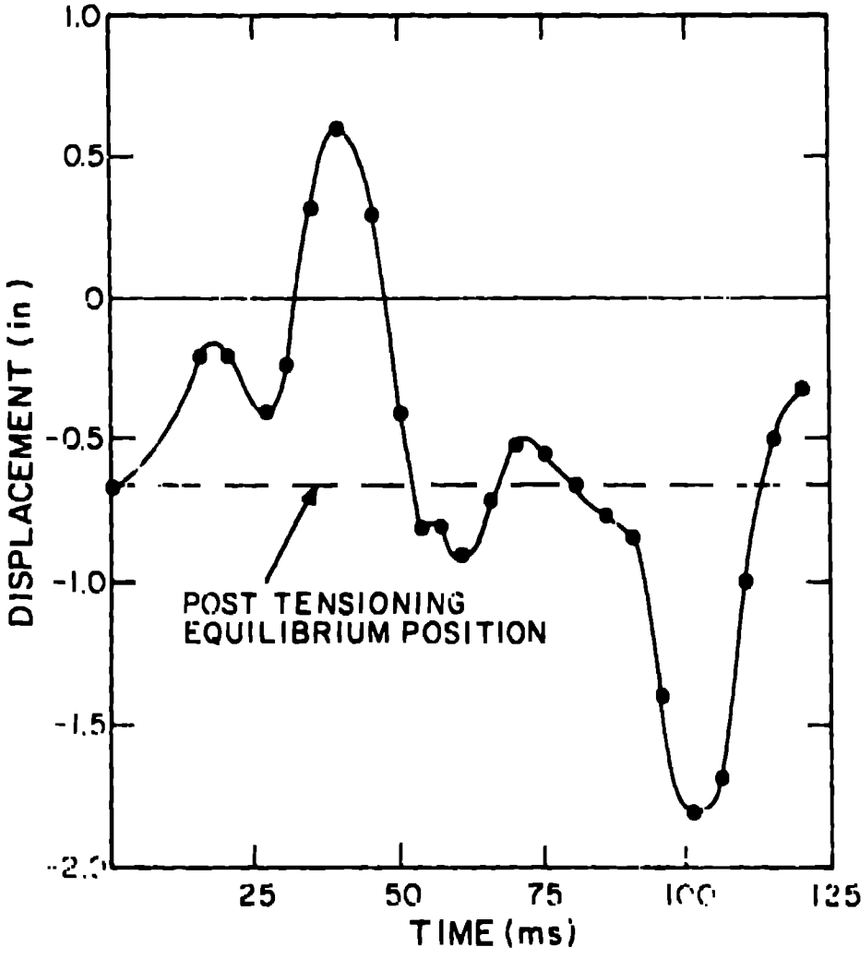
1.0
0.5
0
-0.5
-1.0
-1.5
-2.0
DISPLACEMENT (in)
POST TENSIONING
EQUILIBRIUM POSITION
25
50
75
100
125
TIME (ms)

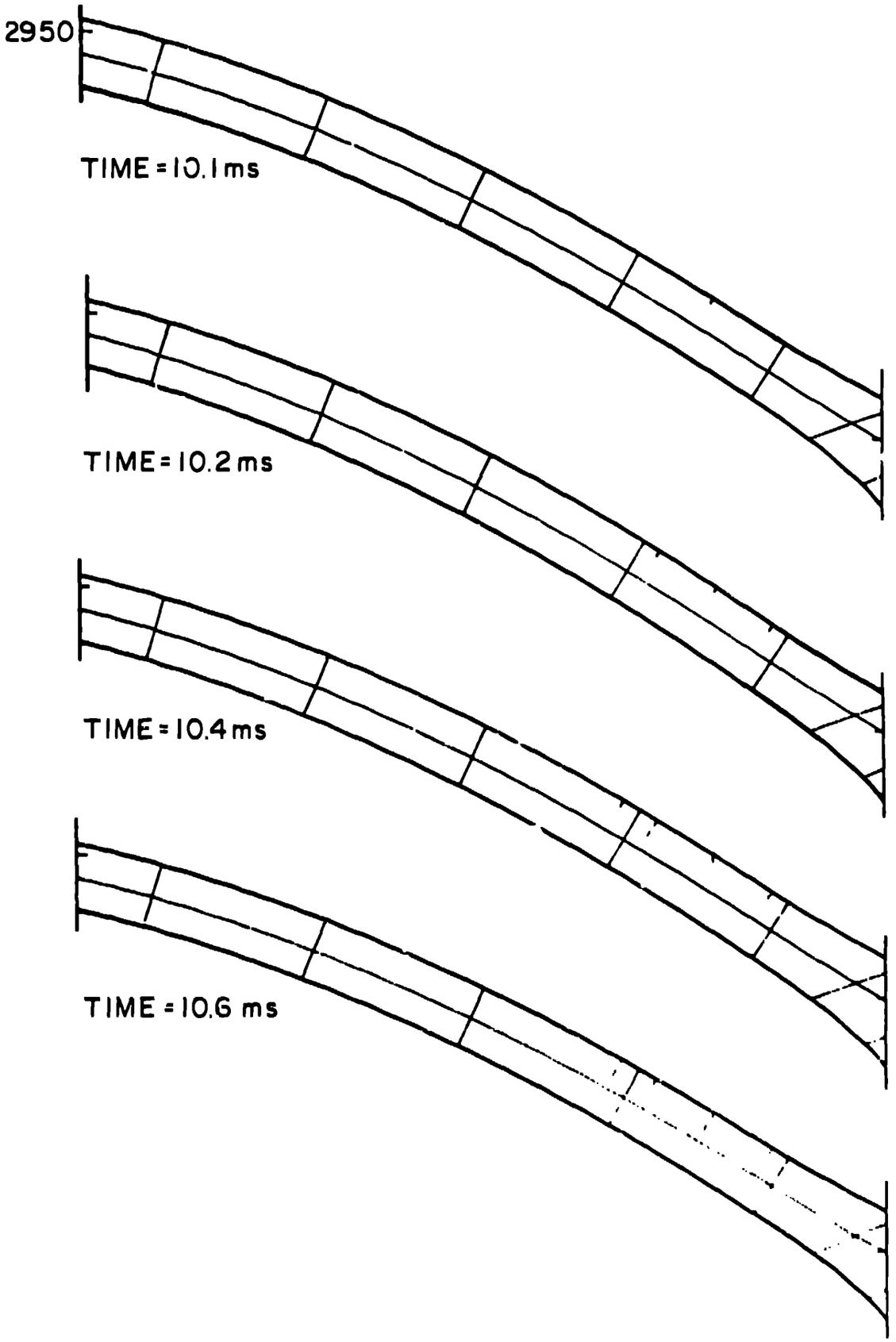
2950
TIME = 10.1 ms
TIME = 10.2 ms
TIME = 10.4 ms
TIME = 10.6 ms

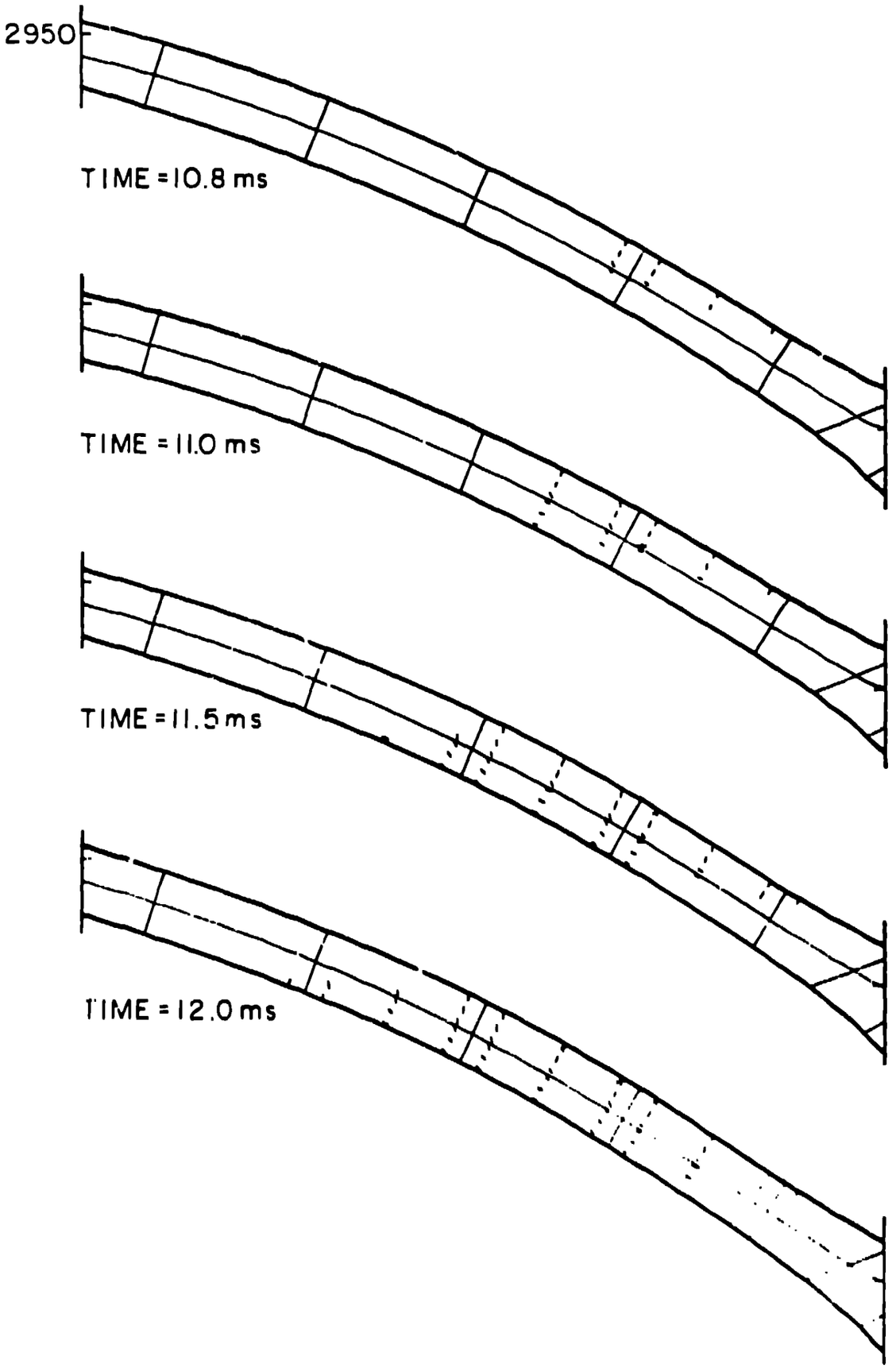
2950
TIME = 10.8 ms
TIME = 11.0 ms
TIME = 11.5 ms
TIME = 12.0 ms

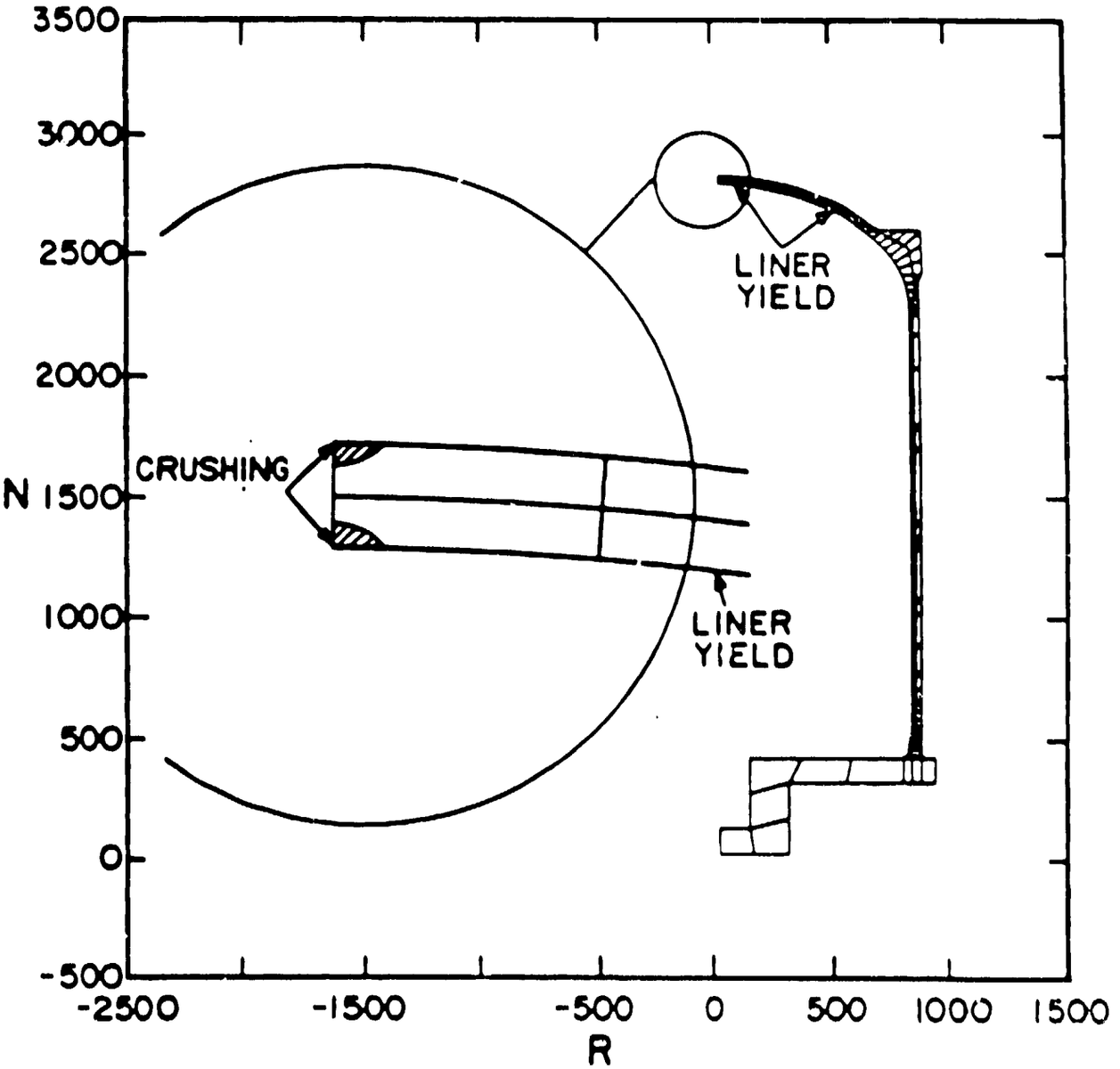
3500
3000
2500
2000
N 1500
1000
500
0
-500
-2500
-1500
-500
0
500
1000
1500
R
LINER
YIELD
CRUSHING
LINER
YIELD

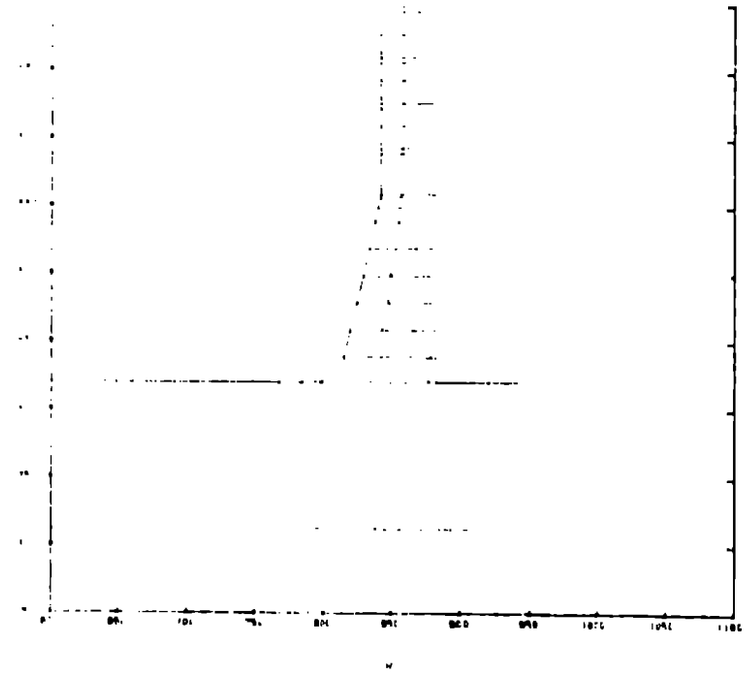

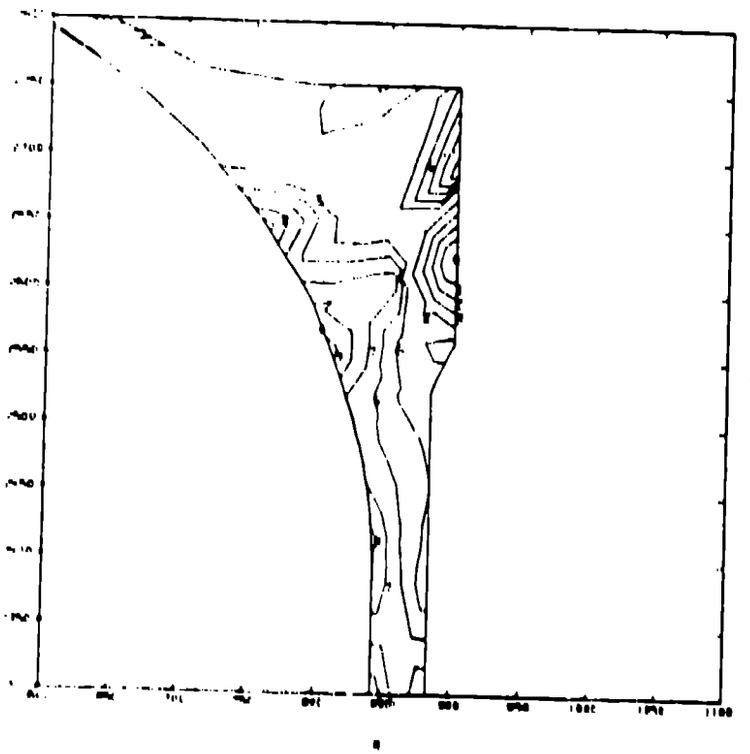

| ND | VALUE |
|---|---|
| * - | 79097E+03 |
| 1 | 711 87 |
| 2 | -519 52 |
| 3 | -327 17 |
| 4 | -134 81 |
| 5 | 57 54 |
| 6 | 112 58 |
| 7 | 167 62 |
| 8 | 222 67 |
| 9 | 277 71 |
| 10 | 332 75 |
| * | 76973E+03 |

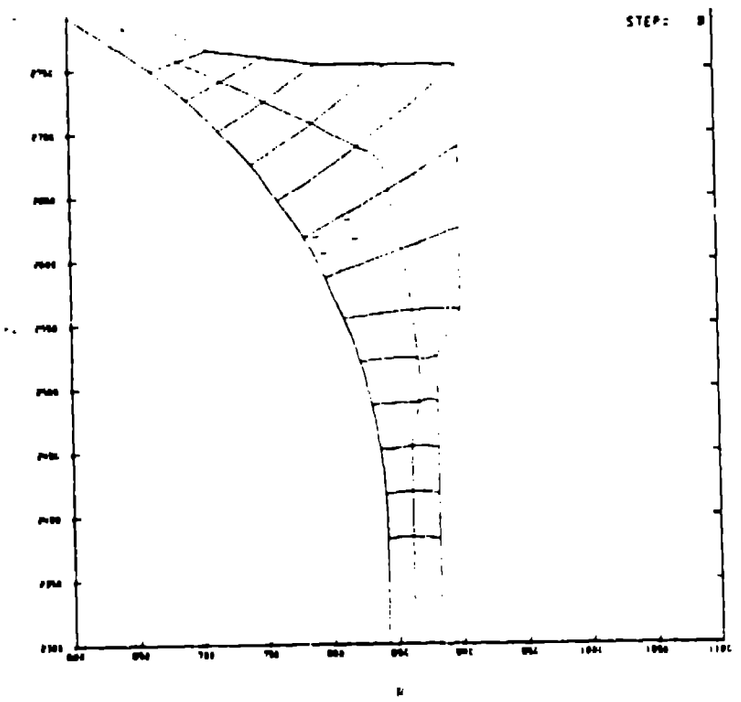
STEP=

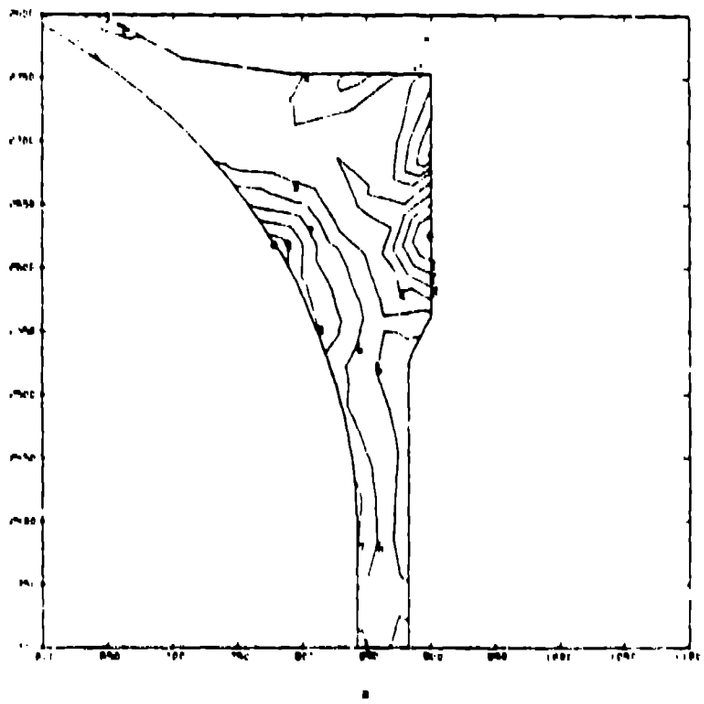
NO VALUE

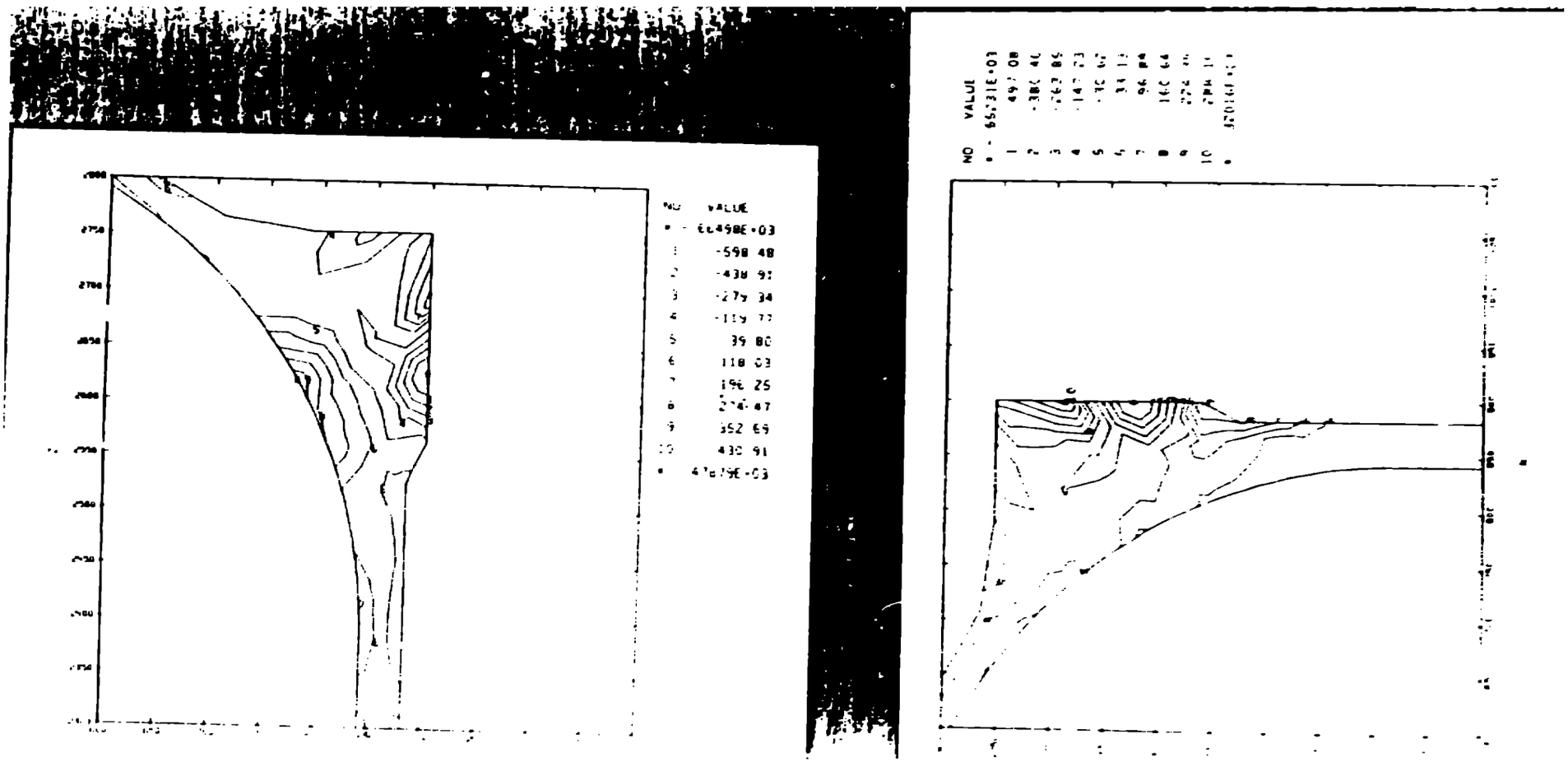
NO VALUE
1 -598.48
2 -438.91
3 -279.34
4 -119.77
5 39.80
6 199.37
7 358.94
8 518.51
9 678.08
10 837.65
NO VALUE
1 496.08
2 -382.41
3 -260.85
4 -139.29
5 -17.73
6 103.84
7 225.40
8 346.96
9 468.52
10 590.08

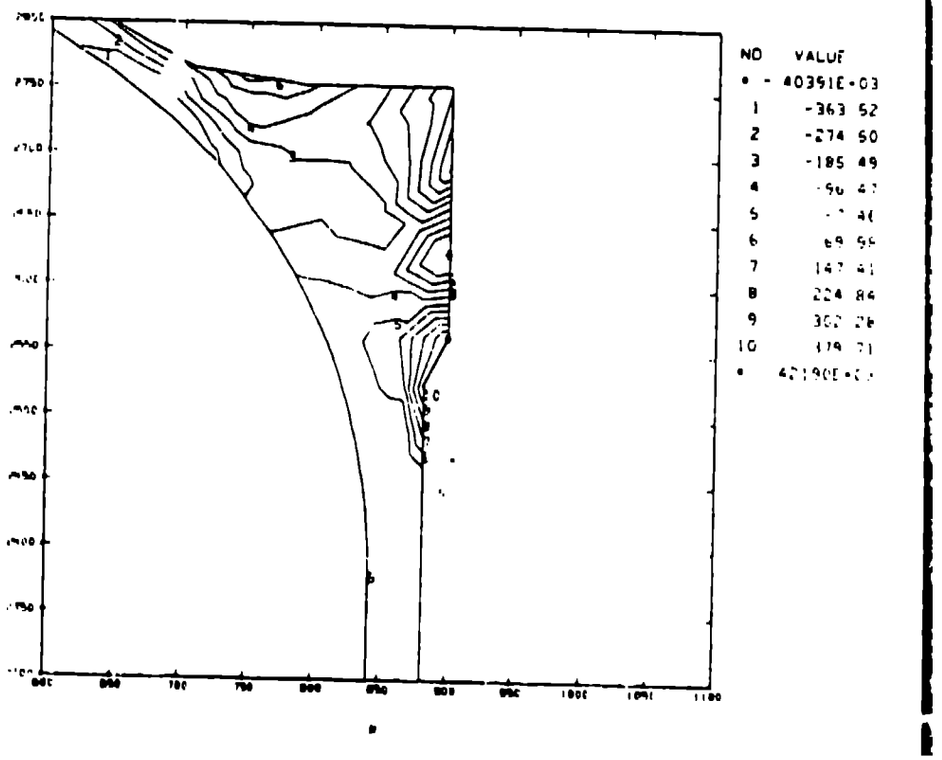

| NO | VALUE |
|---|---|
| * | - 40391E+03 |
| 1 | -363 52 |
| 2 | -274 50 |
| 3 | -185 49 |
| 4 | -96 47 |
| 5 | -7 46 |
| 6 | 82 55 |
| 7 | 171 41 |
| 8 | 260 84 |
| 9 | 349 28 |
| 10 | 438 71 |
| * | 42190E+03 |